



1 **The impact of long-term changes in ocean waves and storm surge on coastal shoreline**
2 **change: A case study of Bass Strait and south-east Australia**

3 Mandana Ghanavati¹, Ian R. Young^{*1}, Ebru Kirezci¹, Jin Liu¹

4 ¹Department of Infrastructure Engineering, University of Melbourne, Melbourne, VIC 3010, Australia.

5 * Corresponding author: ian.young@unimelb.edu.au

6

7 **Abstract**

8 Numerous studies have demonstrated that significant global changes in wave and storm surge
9 conditions have occurred over recent decades. Climate projections indicate such changes are likely
10 to continue out to at least 2100. As coastlines respond to the environmental forcing of waves and
11 storm surges, the question of whether the observed and projected changes in waves and storm
12 surges, will impact coastlines in the future, is important. Previous global-scale analyses of these
13 issues have been inconclusive. This study investigates the south-east coast of Australia over a
14 period of 26 years (1988-2013). Over this period, this area has experienced some of the largest
15 changes in wave climate of any coastal region, globally. The analysis uses high-resolution hindcast
16 data of waves and storm surge, together with satellite observations of shoreline change. All
17 datasets have been previously extensively validated against in situ measurements. The results show
18 that beaches along this region appear to have responded to the increases in wave energy flux and
19 changes in wave direction. This has enhanced non-equilibrium longshore drift and recession of the
20 coastline, with recession rates of up to 1m/year.

21 **1. Introduction**

22 Sandy coastlines are dynamic systems, responding to changes in waves, storm surge, sea level,
23 available coastal sediment supply and human activities (e.g. coastal structures, beach nourishment)
24 (Komar, 1998; Masselink, et al., 2016). These changes occur on a variety of spatial and temporal
25 scales. Spatially, changes in beach alignment and the presence of coastal shoreline features
26 (headlands and bays) impact both the wave climate for individual beaches and the characteristics
27 of longshore drift. At temporal scales of days, beach erosion results from individual storms
28 (Komar, 1998; Harley, et al., 2017; Masselink, et al., 2016). At time scales of 2 to 10 years,
29 changes in storminess associated with climate indices (e.g. El Niño) (Ranasinghe, et al., 2004;
30 Harley, et al., 2011; Barnard, et al., 2015; Vos, et al., 2023) impact beach systems. Longer term
31 changes in mean sea level as a result of climate change are also predicted to result in coastal
32 recession (Hinkel, et al., 2013; Ranasinghe, 2016; Voudoukas, et al., 2020; Ranasinghe, et al.,
33 2021; Vitousek, et al., 2023). It should be noted that throughout this paper we refer to shorter-term
34 changes in beach location due to storms or a series of storms as erosion or accretion. Longer-term
35 changes such as those due to climate change are referred to as recession or progradation.

36 Waves and storm surges are generated by environmental variables (wind and sea level pressure
37 gradient). It has been shown that these environmental variables are impacted by climate change



38 and hence long-term historical changes (trends) in waves (Wang & Swail, 2001; Wang, et al.,
39 2009; Hemer, 2010; Young, et al., 2011; Aydoğan & Ayat, 2018; Zheng & Li, 2017; Young &
40 Ribal, 2019; Takbash & Young, 2020; Reguero, et al., 2019; Cao, et al., 2021) (Young & Ribal,
41 2022; Liu, et al., 2022; Morim, et al., 2022; Erikson, et al., 2022) and storm surges (Paprotny,
42 2014; Androulidakis, et al., 2015; Cid, et al., 2016; Muis, et al., 2016; Kim, et al., 2017; Feng, et
43 al., 2018; Ghanavati, et al., 2023) have been observed. A number of studies have also projected
44 continued global increases (positive trends) in wave height over the 21st century, particularly in
45 the Southern Hemisphere, under plausible climate change scenarios (Hemer, et al., 2013; Meucci,
46 et al., 2020; Hochet, et al., 2021; Liu, et al., 2022; Meucci, et al., 2023; Morim, et al., 2023; Liu,
47 et al., 2023).

48 If sandy coasts are impacted by changes in wave and storm surge conditions, the potential for
49 continued increases in the values of these variables in the future, raises the question as to what
50 impact this may have on sandy coastlines and associated communities. As a means of determining
51 potential future impacts, the obvious precursor is to assess the impacts that historical changes in
52 long-term wave and storm surge conditions have had on coastlines. Ghanavati, et al. (2023) have
53 investigated this issue at global scale by using long-term modelled wave and storm surge data
54 together with satellite observations of beach recession/progradation over the last 30 years. They
55 found that, noting the relatively small trends in wave and storm surge conditions over this period,
56 the accuracy of the available data, and other unrelated impacts on shoreline response (e.g.
57 availability of sediment, human impacts), no clear relationship was evident.

58 The present study extends the Ghanavati, et al (2023) work by examining the south-east coastline
59 of Australia in detail. This is an area where long-term trends in wave conditions are some of the
60 largest in the world, responding to changes in wave climate in the Southern Ocean (Liu, et al.,
61 2022). As a regional area is considered, it is possible to use higher resolution data (both model and
62 satellite) removing uncertainties in the global-scale Ghanavati, et al (2023) study.

63 The structure of the paper is as follows. Section 2 outlines the study area, data sets and analysis
64 techniques used in the study. Results are given in Section 3, including the observed relationships
65 between changes in wave and storm surge quantities and beach recession/progradation. Discussion
66 and conclusions are provided in Section 4.

67

68 **2. Methodology**

69

70 **2.1 Study Area**

71 The study region is shown in Figures 1 and 2, and covers an area of 137E°–155°E, 35S°–45°S.
72 Three Australian coastal states span this domain, Victoria, southern New South Wales and the
73 island of Tasmania in the south of the domain. The south-eastern coast of the mainland of Australia
74 (Victoria), the coastal area of the study, is separated from Tasmania by the relatively shallow Bass
75 Strait. The area is exposed to a particularly complex wave climate (Liu, et al., 2022). To the west,



76 the coast is exposed to the Southern Ocean and hence experiences a very energetic wave climate
77 with recorded significant wave height as high as 10m (Meucci, et al., 2023). The wave climate of
78 this region is dominated by south-westerly Southern Ocean swell. Central regions of the study
79 domain are protected by the island of Tasmania and have a mixed wave climate with swell from
80 both the south-west and south-east and locally generated wind sea. To the east, the wave climate
81 is more heavily dependent on the local wind-sea but with south-easterly swell still playing a role
82 (Liu, et al., 2022).

83

84 Both observational data from satellite altimeters (Young, et al., 2011; Young & Ribal, 2019;
85 Timmermans, et al., 2020) and model hindcasts (and reanalyzes) (Cao, et al., 2021; Young &
86 Ribal, 2022) show that over the last 35 years, there has been a small global increase in mean
87 significant wave height. This increase is largest in the Southern Ocean (approximately 3mm/year
88 or an increase of 3% over the last 30 years), which results in impacts across the Indian, South
89 Pacific and South Atlantic Oceans due to radiating swell. Therefore, the study area is a location
90 where relatively large changes in significant wave height have occurred over the period.

91

92 2.2 Datasets

93 This study uses regional datasets for each of wave, storm surge, and coastal change from which
94 the historical trend magnitudes of the various quantities were calculated. The datasets under
95 consideration cover different periods of time, and thus, to ensure consistency across analyses, a
96 common time period from 1988 to 2013 was selected. A description of each dataset used in the
97 study is provided below.

98

99 *Liu et al. (2022) regional wave hindcast* is a high-resolution regional wave hindcast dataset based
100 on a WAVEWATCH III model with an ST6 physics package (Liu, et al., 2021). The regional
101 model covers the domain shown in Figure 2 using an unstructured grid with a coastal resolution
102 as small as 500m and a coarser deep water resolution as large as 10km. The regional model is
103 nested within a global model using the same ST6 physics (Liu, et al., 2021). Both the regional and
104 global models are forced with ERA5 winds (Hersbach, et al., 2020). The regional wave model
105 dataset has been extensively validated (Liu, et al., 2022; Liu, et al., 2023) against both a network
106 of coastal buoys and satellite altimeter data. Wave data were available from the hindcast with a
107 temporal resolution of 1 hour. The period of the hindcast was from 1981 to 2020. The dataset's
108 high resolution is particularly important for studying coastal regions, where wave conditions can
109 vary significantly over short distances. Additionally, the long period of coverage allows us to
110 identify and analyze trends in the wave climate over several decades, providing insight into the
111 possible effects of historical climate change on the region.

112

113 *Colberg, et al. (2018) Australian water level hindcast* is a dataset of sea level simulations for the
114 Australian coastline. The dataset was generated using the Regional Ocean Modelling System



115 (ROMS) (Shchepetkin & McWilliams, 2005), which was run in a depth-integrated form on a 5 km
116 resolution grid for the Australian region. Tidal boundary conditions were provided by the global
117 model TPXO7.2 (Egbert & Erofeeva, 2002). The ROMS model was run for the period 1981-2013
118 and was forced with NCEP Climate Forecast System Reanalysis (CFSR) (Saha, et al., 2010) wind
119 and surface pressure data. The model has been validated at 14 tide gauge locations around the
120 Australian coastline (Colberg, et al., 2018). Again, the output was available on an hourly basis.

121 *Bishop-Taylor et al., (2021) Geoscience Australia beach dataset* is a high-resolution regional
122 dataset of shoreline change rate for the coast of Australia. The dataset utilizes a combination of
123 satellite visual data and tidal modelling to map shoreline change, with an along-coast resolution of
124 30m for non-rocky (sandy or muddy) areas. The dataset provides annual values of the shoreline
125 position over the period 1988 to 2019. The dataset has been extensively validated using in-situ
126 measurements, comprising 330 validation transects, each spanning over 10 years of coastal
127 monitoring data (Bishop-Taylor, et al., 2021).

128 **2.3 Trend calculation**

129 Each of the datasets (waves, storm surge, shoreline location) are defined at different resolution and
130 in different manners (structured and unstructured grids, specific shoreline positions), therefore
131 none of these quantities are co-located. As shown by Ghanavati, et al., (2023) and subsequently
132 confirmed in Figures 3, 4 and 5, trends in both wave height and storm surge quantities generally
133 vary smoothly along extended coastal regions (100s of kilometres). Shoreline
134 recession/progradation rate can, however, vary rapidly in magnitude and sign over relatively short
135 spatial scales (10s of kilometres) (Luijendijk, et al., 2018; Ghanavati, et al., 2023). That is, one
136 beach can be receding whilst the next is prograding. As such, simple scatter plots of rates of change
137 of wave and storm surge quantities verses recession/pogradation rates are not meaningful. Rather,
138 one needs to consider relationships over spatial regions of the coastline. To achieve such an
139 analysis, we divide the study domain in Figure 1 into six regions, each spanning 2° in longitude –
140 (a) 138E°-140E°, (b) 140E°-142E°, (c) 142E°-144E°, (d) 144E°-146E°, (e) 146E°-148E° and (f)
141 148E°-150E° from west to east. These regions span the differing wave climates of the study
142 domain (see Figure 2 and subsequent discussion). For analysis purposes, we present data as
143 follows. Wave quantities are presented both as colour shaded plots, and at shoreline locations
144 corresponding to ocean points defined by the unstructured WAVEWATCH III computational grid.
145 Storm surge quantities are shown at the locations corresponding to the ocean points nearest the
146 land/sea transition of the ROMS 5km computational grid. Coastal change points are as defined at
147 coastal locations in the Bishop-Taylor et al., (2021) dataset, which has an along-cost resolution of
148 30m.

149 Each of the three datasets used in the study covers a different period of time: wave hindcast - 1981
150 to 2020, storm surge data - 1981 to 2013, and shoreline change data - 1988 to 2019. To ensure a
151 consistent evaluation of the trends and variability in the oceanic parameters, a common analysis
152 period of 1988 to 2013 was selected for the study.



153 For each of the datasets, a range of quantities to be investigated were calculated. These include:
154 waves – mean significant wave height (H_s), 95th percentile significant wave height (H_s^{95}), mean
155 wave energy flux ($C_g E$), mean wave period (T_m) and mean wave direction (θ_m), where C_g is the
156 group velocity of waves and $E = H_s^2 / 16$ is the wave energy. The hourly data from the regional
157 wave model was used to calculate annual values of each of these quantities.

158 As noted above, various datasets have different temporal and spatial resolutions and hence slightly
159 different approaches were used to evaluate the variability and extremes of oceanic parameters. The
160 wave and surge time series were collected at a temporal resolution of 1 hour, while the shoreline
161 dataset provided annual shoreline change with reference to the shoreline location in 2019.
162 Therefore, annual mean values of wave parameters including significant wave height, wave energy
163 flux, wave direction and wave period were calculated. Furthermore, the extremes were determined
164 by calculating annual higher percentiles (95th, 98th, and 99th) for significant wave height and
165 surge level. These metrics provide a consistent basis for evaluating the variability and extremes of
166 the oceanic parameters across different datasets. As the various percentile thresholds gave similar
167 results, extreme events were determined as occasions on which the time series exceeded the 95th
168 percentile but with such events separated by a minimum of 48 hours. The number of such events
169 in each year were defined as $N_{H_s^{95}}$. In a similar fashion, storm surges were defined as occasions
170 when the water surface elevation, η , exceeded the 95th percentile (η^{95}) and the number of such
171 events was defined as $N_{\eta^{95}}$. Again, annual values of these quantities were determined. The annual
172 values of shoreline position from the Bishop-Taylor et al. (2021) data were defined in a similar
173 manner and represented as C_{GA} .

174 The annual values of each quantity were then used to determine linear trends over the period 1988-
175 2013. Both linear regression and the non-parametric Tiel-Sen estimator (Sen, 1968) were used for
176 this purpose. As the resulting values were very similar, the Sen slope estimates are used in the
177 subsequent analysis. The resulting trend values are represented as: ΔH_s , ΔH_s^{95} , $\Delta C_g E$, $\Delta \theta_m$,
178 $\Delta N_{H_s^{95}}$; $\Delta \eta^{95}$, $\Delta N_{\eta^{95}}$; ΔC_{GA} .

179

180 3. Results

181 3.1 Wave climate

182 Figure 2 shows the mean wave climate of the study area and how it has changed over the period
183 1988 to 2013 as indicated by the Liu, et al. (2022) hindcast. Figures 2a and 2b show the mean
184 significant wave height \bar{H}_s and wave energy flux, $\overline{C_g E} = \rho g^2 H_s^2 T_m / (64\pi)$, respectively. As
185 noted above, the significant wave height and wave energy flux vary significantly across the study
186 area. In the west, the coastline is exposed to energetic Southern Ocean swell with mean H_s of
187 approximately 3m. In the eastern regions of the study area, where there is protection provided by



188 the island of Tasmania, mean H_s decreases significantly to less than 1.5m, a decrease by a factor
189 of approximately 2. The wave energy flux shows an even more significant change, with mean
190 values varying from approximately 60kW/m in the west to 15kW/m in the east, a factor of 4. The
191 substantial reduction in wave energy flux is attributed to the protection provided by the island of
192 Tasmania, which leads to a decrease in both H_s and T_m . As shown by Liu, et al. (2022), the
193 mean/peak wave direction also changes significantly across the domain. In the west, the dominant
194 wave direction is defined by energetic south-westerly swell. In the east, the protection provided by
195 the island of Tasmania means that swell entering the area is predominately from the south-east.

196 The changes in wave climate over the study period are also significant across this region. As noted
197 above, a range of studies have shown that the Southern Ocean wave climate has increased over the
198 past 35 years (Young, et al., 2011; Young & Ribal, 2019; Cao, et al., 2021; Young & Ribal, 2022).
199 Swell from the Southern Ocean dominates the western areas of the study region and hence there
200 have been significant changes in the wave climate, as shown by Figures 2c-h. In the west, H_s has
201 increased by approximately 5% (Figure 2c) over the study period and $C_g E$ by approximately 14%
202 (Figure 2d). In contrast, in the east, where the wave climate is not as exposed to Southern Ocean
203 swell, these values decrease to approximately zero (no change). Figures 2e and f clearly show that
204 the positive trends in H_s are due to changes in both swell and local wind-waves. Figure 2g also
205 shows that there have been only small changes in T_m across the domain.

206 The most dramatic changes in wave climate concern the mean wave direction, θ_m . Over the
207 western regions of the study domain, there has been a small counter-clockwise rotation of the mean
208 wave direction (less than 1.5°). This is a result of the gradual southward movement of Southern
209 Ocean low pressure systems over recent decades (Morim, et al., 2022). This small change in deep
210 water wave direction, significantly impacts the shadow region in the lee of Tasmania and hence
211 the wave direction, resulting in much larger counter-clockwise rotations of approximately 5°
212 (Figure 2h). These values reduce towards the coast of mainland Australia (eastern area of study
213 region) but are still larger than 3° .

214 3.2 Storm Surge Climate

215 As noted above, storm surges were defined as events where the water surface elevation exceeded
216 the 95th percentile value, η^{95} . Figure 3 and 4 show plots for each of the sub-regions referenced in
217 Figure 1. These figures show colour contoured values of $\Delta C_g E$ (Figure 3) and $\Delta \theta_m$ (Figure 4),
218 coastal values of $\Delta \eta^{95}$ and ΔC_{GA} . In contrast to the wave climate, changes in storm surge, $\Delta \eta^{95}$
219 are very consistent along the coastline of the study area. Values of $\Delta \eta^{95}$ are negative along the
220 entire coastline, decreasing in magnitude from approximately -0.3cm/year in the west to
221 -0.2cm/year in the east. The fact that the magnitude of storm surges has been decreasing over this
222 period is consistent with the observations of Liu, et al. (2023) that as Southern Ocean low pressure



223 systems move south, they increase the mean atmospheric pressure and reduce the pressure gradient
224 over southern Australia. As surface pressure (and wind) drives storm surge, this results in a
225 tendency for a reduction in the magnitude of storm surges.

226

227 3.3 Relationship between waves, storm surge and shoreline change

228 As previously shown at global scale by Luijendijk, et al. (2018) and Ghanavati, et al. (2023),
229 recession/progradation rates vary in magnitude and sign on relatively small spatial scales. This is
230 because sediment transport can be both offshore/onshore as well as longshore. In the case of non-
231 equilibrium longshore transport of sediment, one would expect some beaches to recede whilst
232 other receive sediment from these beaches and hence prograde. Ghanavati, et al. (2023) speculated
233 that coastlines which show such non-equilibrium behaviour may be responding to long-term
234 changes in the environmental forcing provided by trends in waves and storm surge. A causal
235 relationship is, however, complicated by other variables which may have a larger impact on beach
236 position. These additional factors include the availability of sediment supplied to beach
237 compartments from fluvial sources and the impacts of human-induced interventions such as coastal
238 structures and beach nourishment (Ranasinghe, 2016). Ghanavati, et al. (2023) limited
239 recession/progradation data to values in the range $\pm 1\text{m/year}$ to confine the datasets to changes
240 which may be a result of long-term processes rather than fluvial and human-induced influences,
241 which tend to be much larger in magnitude (Luijendijk, et al., 2018).

242 Therefore, following these precedents, in Figures 3 – 6, the quantity ΔC_{GA} has been filtered to retain
243 only values in the range $\pm 1\text{m/year}$. Figure 5 shows values of ΔC_{GA} (in the range $\pm 1\text{m/year}$) as a
244 bar chart along the coastline from 138E° to 150E° . Each of the 2° regions shown in Figures 1, 4
245 and 5 is marked along the longitude axis. As expected, values of ΔC_{GA} in Figures 3, 4 and 5 show
246 both positive (progradation) and negative (recession) values. To quantify recession/progradation,
247 values of ΔC_{GA} in the range -0.05m/year to -1.00m/year are classified as recession, values in the
248 range $+0.05\text{m/year}$ to $+1.00\text{m/year}$ as progradation and values in the range $\pm 0.05\text{m/year}$ as
249 representing stable coastlines. Table 1 shows the percentage of coastal locations classified as
250 receding, prograding or stable under these criteria. In addition, Figure 6 shows histograms of the
251 distribution of the magnitudes of the values of ΔC_{GA} .

252 Table 1 and Figure 6 show that the sections (c) 142E° - 144E° and (f) 148E° - 150E° are
253 predominately receding. Segment (d) 144E° - 146E° shows quite large values of both recession and
254 progradation (see Figure 5) but with more locations prograding than receding. However, this
255 region is complicated by the presence of Port Phillip Bay. The other segments (a), (b) and (e)
256 show no clear difference between the percentage of receding and prograding locations.

257 To understand the results shown in Table 1, we consider each of the two degree sections shown in
258 Figures 3, 4 and 5. In these figures, values of the trend in wave energy flux, $\Delta C_g E$ (Figure 3) or



259 wave direction, $\Delta\theta_m$ (Figure 4) are shown as colour shaded contours over the regions. The trend
260 in storm surge (always negative) are shown as colour coded squares at 5km intervals along the
261 shoreline, at the resolution of the water level model. The satellite-derived values of trend in
262 shoreline location at each beach location (Bishop-Taylor, et al., 2021) are shown as colour coded
263 filled circles, at the 30m along-coast resolution.

264 Figures 3a and 4a show the region from 138E° to 140E° (segment (a), Victor Harbour to Cape
265 Jaffa). This region shows relatively small positive values of $\Delta C_g E$ (approximately 0.01kWm⁻²
266 ¹/year) and a small counter-clockwise rotation of the mean wave direct (approximately
267 -0.02deg/year or 0.6° over 30 years). In response to these small changes in wave properties there
268 is no consistent changes in shoreline. In the western regions (138.6E°-139.2E°) the shoreline is
269 prograding. However, this may be associated with fluvial sediments, as this region is the ocean
270 entrance of Lake Alexandrina and the mouth of the Murray River. These results are consistent with
271 the bar chart of Figure 5 and the results in Table 1 and Figure 6a that there is no clear difference
272 between recession and progradation for segment (a).

273 Moving east to segment (b), values of $\Delta C_g E$ increase (Figure 3b) and the region shows small
274 receding shorelines (139.6E°- 141.0E°). This changes to progradation between 141.0E°-141.2E°,
275 west of Cape Bridgewater. This behaviour is consistent with sediment being moved along the
276 shoreline west to east from 139.6E°- 141E° by the increasing wave energy flux and the prevailing
277 wave direction from the south-west. This sediment transport is interrupted by Cape Bridgewater
278 resulting in the progradation between 140.8E°-141.2E°. The overall balance between these regions
279 results in no clear difference between locations receding and prograding in Table 1 and Figure 6b.

280 The strong positive trend in wave energy flux is maintained east of Cape Bridgewater (segment
281 (c), Figures 3c) with small counter-clockwise rotation of the mean wave direction (Figure 4c).
282 Along this extended region of the coast to Cape Otway (141.6E°-143.6E°), the coastline shows
283 small recession (approximately -0.1m/year – 3m over the measurement period of 30 years). East
284 of Cape Otway, the magnitude of the recession decreases and the shoreline shows little net change
285 in location. This behaviour is consistent with the reduced impact of south-westerly swell east of
286 Cape Otway, which provides some shelter from such waves. Table 1 and Figure 6c show that
287 summed across the full segment (c), a total of 53% of locations are receding and only 27%
288 prograding.

289 East of Cape Otway, the wave energy flux climate near the coast decreases (Figure 2b), as Cape
290 Otway provides protection from the south-westerly swell and $\Delta C_g E$ also decreases as the
291 protection provided by Tasmania becomes important (Figure 3d). The shoreline trends, ΔC_{GA} , are
292 complicated by the presence of Port Phillip Bay (Figures 3d, 4d). From Cape Otway to Inverloch
293 (143.6E°- 145.8E°) there is relatively little change in ΔC_{GA} . The relatively small region from
294 Inverloch to Wilson's Promontory (145.8E° - 146.4E°) shows a receding shoreline, previously
295 noted in studies of the area (Leach, et al., 2023). As a result, there is no clear overall differences



296 between recession and progradation for this section (Table 1 and Figure 6d). However, if one
297 considers just the ocean beaches (exclude Port Phillip Bay in Figures 3d and 4d), then there is
298 small recession along the entire coastline of section (d).

299 East of Wilson's Promontory the coastline is characterized by very long beaches and barrier islands
300 (Ninety-mile beach). This region from 147°E to 149.6°E (Wilson's Promontory to Cape Howe)
301 (Figures 3e-f, 4e-f) is characterized by a large counter-clockwise rotation of the mean wave
302 direction. The region immediately east of Wilson's Promontory ($146.5^{\circ}\text{E} - 147^{\circ}\text{E}$) shows strong
303 progradation. The remainder of this extended coastline, however, shows consistent recession of
304 approximately -0.5m/year (15m over the measurement period), particularly for section (f). This
305 section shows the strongest recession of any extended section, with Table 1 showing 60% of
306 locations receding and only 30% prograding. As noted above, the dominant swell in this region is
307 from the south-east and, although the changes in wave energy flux are small, there has been a
308 significant counter-clockwise rotation of the wave direction over the study period. This results in
309 the wave direction gradually becoming more shore-parallel. Therefore, the shoreline change noted
310 above is consistent with an increase in longshore drift (east to west) with sediment being
311 accumulated to the east of Wilson's Promontory. We should also note that this area east of Wilson
312 Promontory is one of the few estuarine environments along the entire Victorian coast and hence
313 some of the observed progradation may be due to fluvial deposits and ebb-tide delta formation
314 (Konlechner, et al., 2020).

315 The results above use the percentage of coastal locations prograding or receding as the measure of
316 whether the beach is responding to long term changes in waves and/or storm surge. As such, it
317 does not consider the magnitudes of the progradation or recession. Figure 6 shows histograms of
318 the magnitudes of the progradation/recession rates for each coastal sections. The figure confirms
319 the results above showing sections (c) $142^{\circ}\text{E} - 144^{\circ}\text{E}$ and (f) $148^{\circ}\text{E} - 150^{\circ}\text{E}$ are clearly receding
320 with other sections less clear, as explained for each section above.

321 In the above analysis, we speculate that changes in wave energy flux, $\Delta C_g E$ and mean wave
322 direction, $\Delta \theta$ are the primary drivers of the observed changes in shoreline. The observed data
323 supports this speculation. The Supplementary Material shows plots similar to Figures 3 and 4 for
324 changes in the other related quantities: significant wave height, ΔH_s (Figures S1 a-c and S1 d-f),
325 extreme significant wave height, ΔH_s^{95} (Figures S2 a-c and S2 d-f), mean wave period, ΔT_m
326 (Figures S3 a-c and S3 d-f) and number of extreme wave events, $\Delta N_{H_s^{95}}$ (Figures S4 a-c and S4 d-
327 f).

328

329 4. Discussion and conclusions

330 Ghanavati, et al. (2023) found that at global scale, they could not distinguish a clear relationship
331 between modelled (and observed) changes in wave energy flux and storm surge over the last 30



332 years and changes in shoreline position. The present dataset extends this result by considering the
333 region of south-east Australia. This region is important in that it is an area with major spatial
334 variations in wave energy flux climate (mean conditions) and some of the largest coastal trends in
335 wave energy flux and mean wave direction globally in the last 30 years. In addition, both high
336 resolution coastal wave and storm surge hindcasts are available, as well as high resolution
337 observations of shoreline change. As such, this is a unique region to determine if observable
338 changes in shoreline position are evident as a consequence of long term changes in wave (and/or
339 storm surge) climate.

340 The results show clear changes in shoreline position, which are consistent with positive trends in
341 wave energy flux and changes in mean wave direction. In the western regions of the domain the
342 mean wave direction is from the south-west and there have been positive trends in wave energy
343 flux, $\Delta C_g E$ of approximately 14% (6/43kW/m). This appears to have resulted in non-stationary
344 longshore drift from west to east and shoreline changes of approximately 3m over the 30 year
345 study period.

346 In the central regions of the study domain both the mean wave energy flux and trends in wave
347 energy flux decrease, as the island of Tasmania provides protection from the south-westerly swell.
348 In this region there are no consistent trends in shoreline position with a similar number of coastal
349 locations receding and prograding. Although ocean beaches do show small recession.

350 To the eastern end of the study domain, the protection provided by Tasmania and the deepwater
351 counter-clockwise rotation of the mean wave climate means that the wave shadow of Tasmania
352 results in a relatively large counter-clockwise rotation of the mean wave direction (up to 6° over
353 the last 30 years). These changes in mean wave direction appear to be driving non-stationary
354 behaviour of the beach systems in the region with the coastline from 146° to 149° (approximately
355 300 km) receding by up to 30m over the 30 year study period.

356 The results presented in this analysis are consistent with a study of this same region by Konlechner,
357 et al. (2020) using lower resolution shoreline change data (Luijendijk, et al., 2018). The shoreline
358 change “hot-spots” of that study are consistent with the present results. The results of the present
359 study are also consistent with the global findings of Ghanavati, et al. (2023). Here, we find that
360 long term changes in wave climate can apparently drive long-term changes in beach location but
361 that relatively large changes in wave energy flux and/or direction are required to produce
362 measurable changes in beach position. As noted, the study region has both a very energetic wave
363 climate and some of the largest trends in this climate of any coastline.

364 Even in such a region, the observed changes in wave climate over the last 30 years are such that
365 the resulting changes in beach location are not large (up to 1.0 m/year or 30m over the study
366 period).

367 In the present analysis, we speculate that the observed changes in shoreline position in the western
368 section of the domain are driven by non-stationary longshore drift from west to east with sediment



369 transport being intercepted by Cape Bridgewater. Such behaviour is consistent with the observed
370 increases in wave energy flux and the predominately south-westerly swell. In the eastern sections
371 of the domain, we speculate that there is sediment transport from the east to west, intercepted by
372 Wilson's Promontory. This speculation is consistent with the predominately south-easterly swell
373 in the region and the observed counter-clockwise change in mean wave direction over the study
374 period.

375 Although such speculation is consistent with the datasets, other processes may also have an impact
376 on shoreline change. The most obvious such changes is sea level rise, which could be expected to
377 cause shoreline recession. Observations (Watson, et al., 2015; Nerem, et al., 2018) indicate that in
378 recent years sea level rise in the Australia region has been approximately 3mm/year. The bed slope
379 along the south-eastern coast of Australia is on average approximately 1:100 (Athanasiou, et al.,
380 2019). Therefore, application of Bruun's rule (Bruun, 1962) would suggest a uniform recession of
381 approximately 0.3 m/year. Such a value is smaller than, but comparable, to the observed recession
382 in the western and eastern portions of the study domain. Recession due to sea level rise, however,
383 would not account for the observed progradation west of Cape Bridgewater or east of Wilson's
384 Promontory. In addition, Bishop-Taylor, et al. (2021) indicate that over their full dataset for
385 Australia, approximately the same number of beaches are receding (11.1%) as prograding (11.0%).
386 Table 1 indicates that for the present study region this is also the case. Sea level rise would be
387 expected to result in a net recession of beaches. In contrast non-equilibrium longshore drift driven
388 by changes in wave climate will cause some beaches to recede whilst other prograde.

389 Therefore, we conclude that the present results are more consistent with the impacts of changes in
390 wave climate rather than sea level rise. Of course, sea level rise will undoubtedly have a major
391 impact in coming years.

392

393 **Code/Data availability**

394 All data used in the paper and codes for the analysis are available from the authors upon request.

395

396 **Competing Interests**

397 The authors declare no competing interests.

398

399 **Author Contributions**

400 MG: Data curation, Investigation, Writing – original draft, Writing – review and editing; IY:
401 Conceptualization, Investigation, Supervision, Writing – original draft, Writing – review and
402 editing; EK: Writing – review and editing; JL: Writing – review and editing



403 **References**

- 404 Androulidakis, Y. S. et al., 2015. Storm surges in the Mediterranean Sea: variability and trends
405 under future climatic conditions. *Dynamics of Atmospheres and Oceans*, Volume 71, pp. 56-82.
- 406 Athanasiou, P. et al., 2019. Global distribution of nearshore slopes with implications for coastal
407 retreat. *Earth System Science Data*, Volume doi.org/10.5194/essd-2019-71.
- 408 Aydođan, B. & Ayat, B., 2018. Spatial variability of long-term trends of significant wave heights
409 in the Black Sea. *Applied Ocean Research*, Volume 79, pp. 20-35.
- 410 Barnard, P. et al., 2015. Coastal vulnerability across the Pacific dominated by El Niño/Southern
411 Oscillation. *Nature Geosciences*, Volume 8, p. 801–807.
- 412 Bishop-Taylor, R., Nanson, R., Sagar, S. & Lymburner, L., 2021. Mapping Australia's dynamic
413 coastline at mean sea level using three decades of Landsat imagery. *Remote Sens. Environ.*,
414 Volume 267, p. 112734.
- 415 Bruun, P., 1962. Sea-Level Rise as a Cause of Shore Erosion. *Proc. American Society of Civil*
416 *Engineers*.
- 417 Cao, Y., Dong, C., Young, I. & Yang, Y., 2021. Global wave height slowdown trend during a
418 recent global warming slowdown. *Remote Sensing*, Volume 13, p. 4096.
- 419 Cid, A. et al., 2016. Long-term changes in the frequency, intensity and duration of extreme storm
420 surge events in southern Europe. *Climate Dynamics*, 46(5), p. 1503–1516.
- 421 Colberg, F., McInnes, K., O'Grady, J. & Hoeke, R., 2018. CSIRO Australia Coastal Sealevel
422 Simulations. v1. CSIRO. Data Collection. p. <https://doi.org/10.4225/08/5a7280a3a0d2a>.
- 423 Egbert, G. D. & Erofeeva, S. Y., 2002. Efficient inverse modeling of barotropic ocean tides. *J.*
424 *Atmos. and Ocean. Tech.*, Volume 19, p. 183–204.
- 425 Erikson, L. et al., 2022. Global ocean wave fields show consistent regional trends between 1980
426 and 2014 in a multi-product ensemble. *Comms. Earth & Env.*, Volume 3, p. 320.
- 427 Feng, J. et al., 2018. Storm surge variation along the coast of the Bohai Sea. *Scientific Reports*,
428 8(1), pp. 1-10.
- 429 Ghanavati, M. et al., 2023. An assessment of whether long-term global changes in waves and
430 storm surges have impacted global coastlines. *Scientific Reports*, Volume 13, p. 11549.
- 431 Harley, M. D. et al., 2017. Extreme coastal erosion enhanced by anomalous extratropical storm
432 wave direction. *Sci. Rep.*, Volume 7, p. 6033.
- 433 Harley, M., Turner, I., Short, A. & Ranasinghe, R., 2011. A re-evaluation of coastal embayment
434 rotation: The dominance of cross-shore versus alongshore sediment transport processes,
435 Collaroy-Narrabeen Beach, southeast Australia. *Jnl. Geophys. Res. (Earth Surface)*, Volume
436 116.



- 437 Hemer, M., 2010. Historical trends in Southern Ocean storminess: Long-term variability of
438 extreme wave heights at Cape Sorell, Tasmania. *Geophys. Res. Lett.*, Volume 37, p. L18601.
- 439 Hemer, M. et al., 2013. Projected changes in wave climate from a multi-model ensemble. *Nature*
440 *Clim. Change*, Volume 3, pp. 471-476.
- 441 Hersbach, H. et al., 2020. The ERA5 global reanalysis. *Q. J. R. Meteorol. Soc.*, Volume 146, pp.
442 1999-2049..
- 443 Hinkel, J. et al., 2013. A global analysis of erosion of sandy beaches and sea-level rise: An
444 application of DIVA. *Global and Planetary Change*, Volume 111, pp. 150-158.
- 445 Hochet, A. et al., 2021. Sea state decadal variability in the North Atlantic: a review. *Climate*,
446 Volume 9, p. 173.
- 447 Kim, D. Y. et al., 2017. Sea Level Rise and Storm Surge around the Southeastern Coast of
448 Korea.. *Journal of Coastal Research*, 79(10079), pp. 239-243.
- 449 Komar, P., 1998. *Beach Processes and Sedimentation*. 544pp ed. s.l.:Prentice Hall.
- 450 Konlechner, T. et al., 2020. Mapping spatial variability in shoreline change hotspots from
451 satellite data; a case study in southeast Australia. *Estuarine, Coastal and Shelf Science*, Volume
452 246, p. 107018.
- 453 Leach, C. et al., 2023. Measuring drivers of shoreline and subaerial beach change using limited
454 datasets in a temperate, wave-dominated sandy system: Inverloch, Australia. *Ocean Coastal*
455 *Management*, Volume 240, p. 106641.
- 456 Liu, J. et al., 2022. The wave climate of Bass Strait and south-east Australia. *Ocean Modelling*,
457 Volume 172, p. 101980.
- 458 Liu, J. et al., 2023. A high-resolution wave energy assessment of south-east Australia based on a
459 40-year hindcast. *Renewable Energy*, Volume 215, p. 118943.
- 460 Liu, J., Meucci, A. & Young, I., 2022. Projected wave climate of Bass Strait and south-east
461 Australia by the end of the twenty-first century. *Climate Dynamics*, pp. 10.1007/s00382-022-
462 06310-4.
- 463 Liu, J., Meucci, A. & Young, I., 2023. Projected 21st Century Wind-Wave Climate of Bass Strait
464 and South-East Australia: Comparison of EC-Earth3 and ACCESS-CM2 Climate Model
465 Forcing. *Jnl. Geophys. Res.*, Volume 128, p. e2022JC018996.
- 466 Liu, Q., Babanin, A., Rogers, E. & Zieger, S., 2021. Forty years of global wave hindcasts using
467 the observation-based source terms: validation and geophysical applications. *Journal of*
468 *Advances in Modeling Earth Systems*, 13(8).
- 469 Luijendijk, A. et al., 2018. The state of the world's beaches. *Scientific Reports*, Volume 8, pp. 1-
470 11.



- 471 Masselink, G. et al., 2016. Extreme wave activity during 2013/2014 winter and morphological
472 impacts along the Atlantic coast of Europe. *Geophys. Res. Lett.*, Volume 43, p. 2135–2143.
- 473 Meucci, A., Young, I., Hemer, M. K. E. & Ranasinghe, R., 2020. Projected 21st century changes
474 in extreme wind-wave events. *Science Advances*, 6(24), p. eaaz7295.
- 475 Meucci, A. et al., 2023. 140 Years of Global Ocean Wind-Wave Climate Derived from CMIP6
476 ACCESS-CM2 and EC-Earth3 GCMs: Global Trends, Regional Changes, and Future
477 Projections. *Jnl. Climate*, Volume 36, pp. 1605-1631.
- 478 Meucci, A. et al., 2023. Evaluation of spectral wave model physics as applied to a 100-year
479 Southern Hemisphere extra tropical-cyclone sea state. *J. Geophys. Res. Oceans*, Volume 128, p.
480 e2022JC018996.
- 481 Morim, J. et al., 2022. A global ensemble of ocean wave climate statistics from contemporary
482 wave reanalysis and hindcasts. *Scientific Data*, Volume 9, p. 358.
- 483 Morim, J. et al., 2023. Understanding uncertainties in contemporary and future extreme wave
484 events for broad-scale impact and adaptation planning. *Science Advances*, Volume 9, p.
485 eade3170.
- 486 Muis, S. et al., 2016. A global reanalysis of storm surges and extreme sea levels. *Nat. Commun.*,
487 Volume 7, p. 11969.
- 488 Nerem, R. et al., 2018. Climate-change–driven accelerated sea-level rise detected in the altimeter
489 era. *Proc. National Academy of Sciences*, Volume 115, p. 2022–2025.
- 490 Paprotny, D., 2014. Trends in storm surge probability of occurrence along the Polish Baltic Sea
491 coast.. *arXiv preprint arXiv*.
- 492 Ranasinghe, R., 2016. Assessing climate change impacts on open sandy coasts: A review. *Earth-*
493 *Science Reviews*, Volume 160, pp. 320-332.
- 494 Ranasinghe, R., R., M., A., S. & G., S., 2004. The Southern Oscillation Index, Wave Climate,
495 and Beach Rotation. *Marine Geology*, pp. 273-287.
- 496 Ranasinghe, R. et al., 2021. Climate change information for regional impact and for risk
497 assessment. . In: *Climate Change 2021: The Physical Science Basis. Contribution of Working*
498 *Group 1 to the Sixth Assessment Report of the Intergovernmental Panel on Climate Change*.
499 Cambridge: Cambridge University Press, pp. 1767-1926.
- 500 Reguero, B. G., Losada, I. J. & Méndez., F. J., 2019. A recent increase in global wave power as a
501 consequence of oceanic warming.. *Nature communications*, pp. 1-14.
- 502 Saha, S. et al., 2010. The NCEP Climate Forecast System Reanalysis. *B. Am. Meteorol. Soc.*,
503 Volume 91, p. 1015–1057.
- 504 Sen, P., 1968. Estimates of the regression coefficient based on Kendals TAU. *Amer. Stats. Assoc.*
505 *Journal*, pp. 1379-1389.



- 506 Shchepetkin, A. F. & McWilliams, J. C., 2005. The regional oceanic modeling system (ROMS):
507 a split-explicit, free-surface, topography-following-coordinate oceanic model. *Ocean Modeling*,
508 Volume 9, p. 347–404.
- 509 Takbash, A. & Young, I., 2020. Long-term and seasonal trends in global wave height extremes
510 derived from ERA-5 reanalysis data. *J. Mar. Sci. & Eng.*, Volume 8, p. 1015.
- 511 Timmermans, B., Gommenginger, C., Dodet, G. & Bidlot, J.-R., 2020. Global Wave Height
512 Trends and Variability from New Multimission Satellite Altimeter Products, Reanalyses, and
513 Wave Buoys. *Geophys. Res. Lett.*, Volume 47, p. e2019GL086880..
- 514 Vitousek, S. et al., 2023. A model integrating satellite-derived shoreline observations for
515 predicting fine-scale shoreline response to waves and sea-level rise across large coastal regions.
516 *Jnl. Geophys. Res. Earth Surface*, p. e2022JF006936.
- 517 Vos, K., Harley, M., Turner, I. & Splinter, K., 2023. Pacific shoreline erosion and accretion
518 patterns controlled by El Niño/Southern Oscillation. *Nature Geoscience*, Volume 16, p. 140–146.
- 519 Vousdoukas, M. et al., 2020. Economic motivation for raising coastal flood defenses in Europe.
520 *Nature Comms.*, Volume 11, p. 2119.
- 521 Wang, X. L. & Swail, V. R., 2001. Changes of extreme wave heights in northern hemisphere
522 oceans and related atmospheric circulation regimes. *J. Clim.*, pp. 2204–2221.
- 523 Wang, X. L. et al., 2009. Detection of external influence on trends of atmospheric storminess and
524 northern oceans wave heights.. *Clim. Dyn.* , pp. 189–203.
- 525 Watson, C. et al., 2015. Unabated global mean sea-level rise over the satellite altimeter era.
526 *Nature Climate Change*, Volume 5, p. 565–568.
- 527 Young, I. & Ribal, A., 2019. Multi-platform evaluation of global trends in wind speed and wave
528 height. *Science*, Volume 364, pp. 548–552.
- 529 Young, I. & Ribal, A., 2022. Can multi-mission altimeter datasets accurately measure long-term
530 trends in wave height. *Rem. Sens.*, Volume 14, p. 974.
- 531 Young, I., Zieger, S. & Babanin, A., 2011. Global trends in wind speed and wave height.
532 *Science*, Volume 332, pp. 451–455.
- 533 Zheng, C. W. & Li, C. Y., 2017. Analysis of temporal and spatial characteristics of waves in the
534 Indian Ocean based on ERA-40 wave reanalysis.. *Applied Ocean Research*, Volume 63, pp. 217-
535 228.
- 536
- 537
- 538
- 539



540 **Tables and Figures**

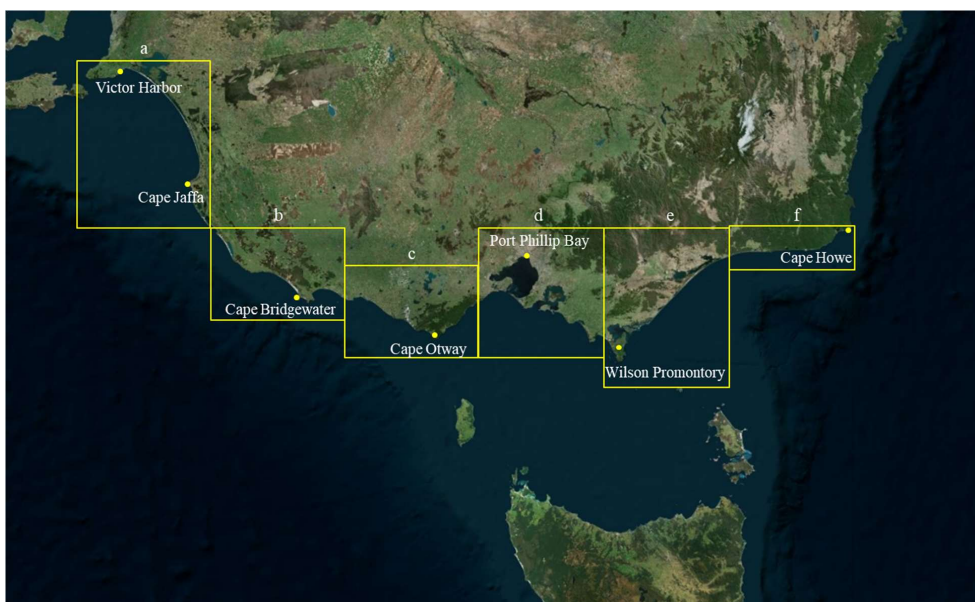
541

Coastal Segment	Recession (-0.05 to -1m/yr)	Progradation (+0.05 to +1m/yr)	Stable (-0.05 to +0.05m/yr)
(a) 138°-140°	40%	45%	15%
(b) 140°-142°	40%	46%	14%
(c) 142°-144°	53%	27%	20%
(d) 144°-146°	37%	49%	14%
(e) 146°-148°	40%	50%	10%
(f) 148°-150°	60%	30%	10%

542

543 Table 1: Percentage of coastal locations, as defined by the Bishop-Taylor, et al. (2021) dataset
544 receding (-0.05 to -1.00m/year), prograding (+0.05 to +1.00m/year) or stable (± 0.05 m/year)
545 over the period 1988 to 2013.

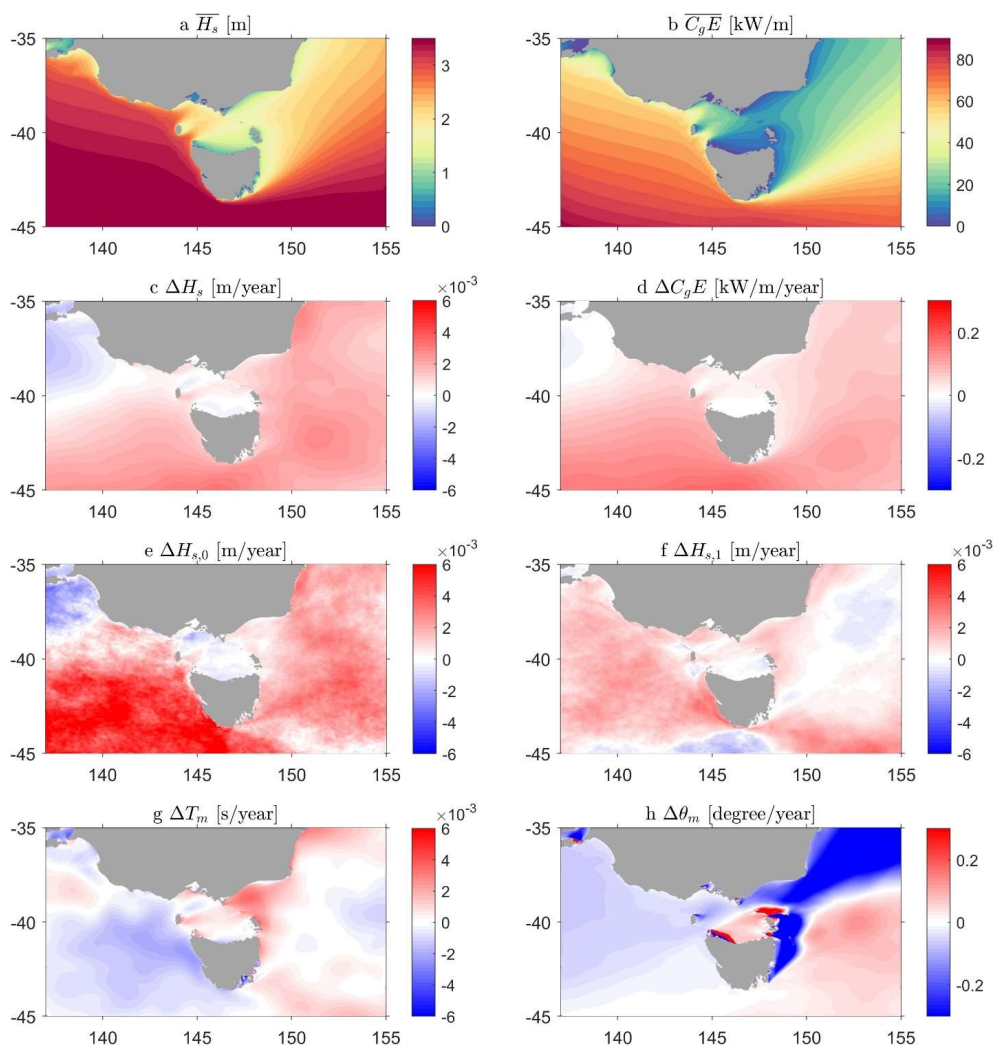
546



547

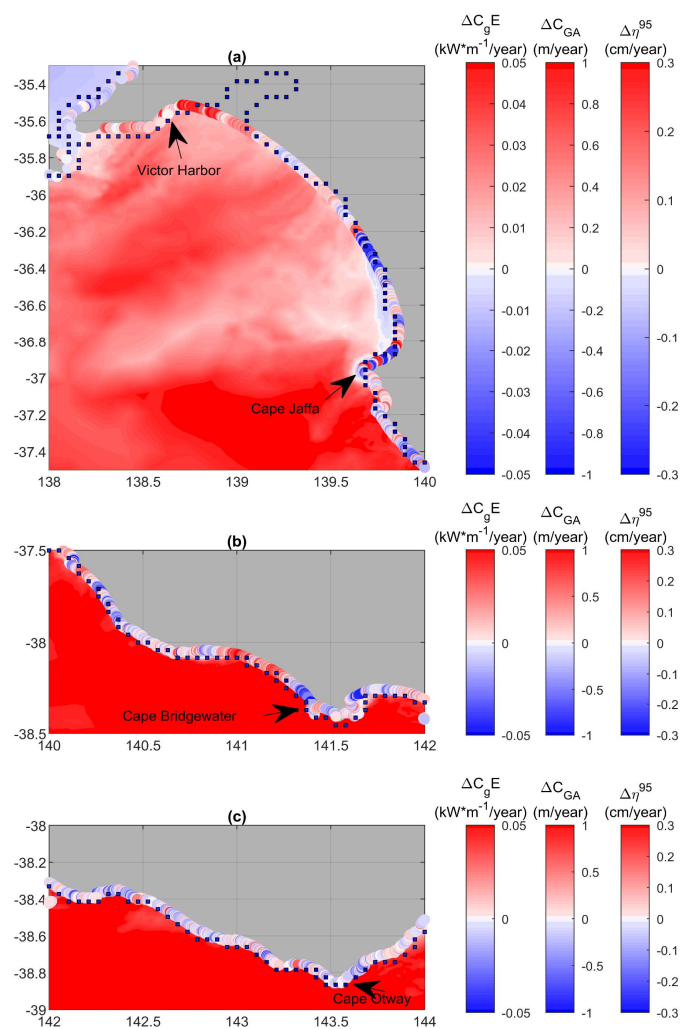
548 Figure 1: The coastal region of south-east Australia comprising the study area. For analysis
549 purposes the region is divided into six sections: (a) 138°-140°, (b) 140°-142°, (c) 142°-144°, (d)
550 144°-146°, (e) 146°-148° and (f) 148°-150° from west to east. The island of Tasmania is to the
551 south of this coastline. (© Google Maps)

552



553

554 Figure 2: Wave climate and trends in the study region of south-eastern Australia over the period
555 1988 to 2013 as modelled by the Liu, et al. (2022) regional wave model. (a) mean significant
556 wave height, (b) mean wave energy flux, (c) trend in significant wave height, (d) trend in wave
557 energy flux, (e) trend in wind-wave portion of the spectrum, (f) trend in swell portion of the
558 spectrum, (g) trend in mean wave period, (h) trend in mean wave direction.

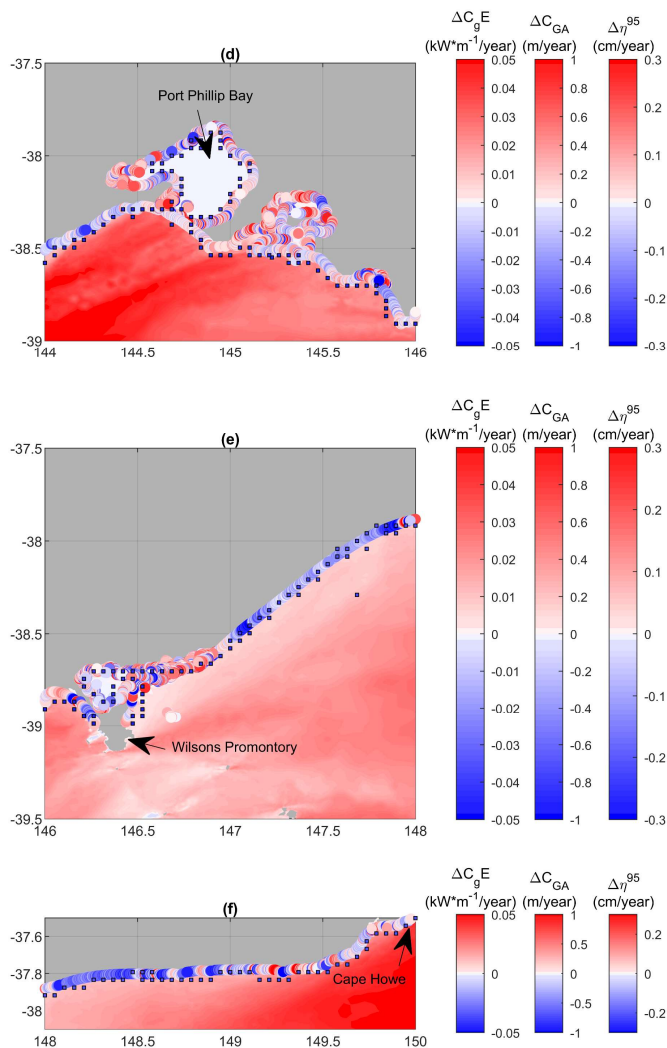


559

560 Figure 3 a-c: Trends in: wave energy flux, $\Delta C_g E$ shown as colour shaded values over the
561 domain, storm surge, $\Delta \eta^{95}$ shown as colour shaded squares at coastal model locations and
562 shoreline progradation/recession, ΔC_{GA} shown as colour shaded circles at beach locations.
563 Results shown for sections (a) 138E°-140E°, (b) 140E°-142E°, (c) 142E°-144E°.



564

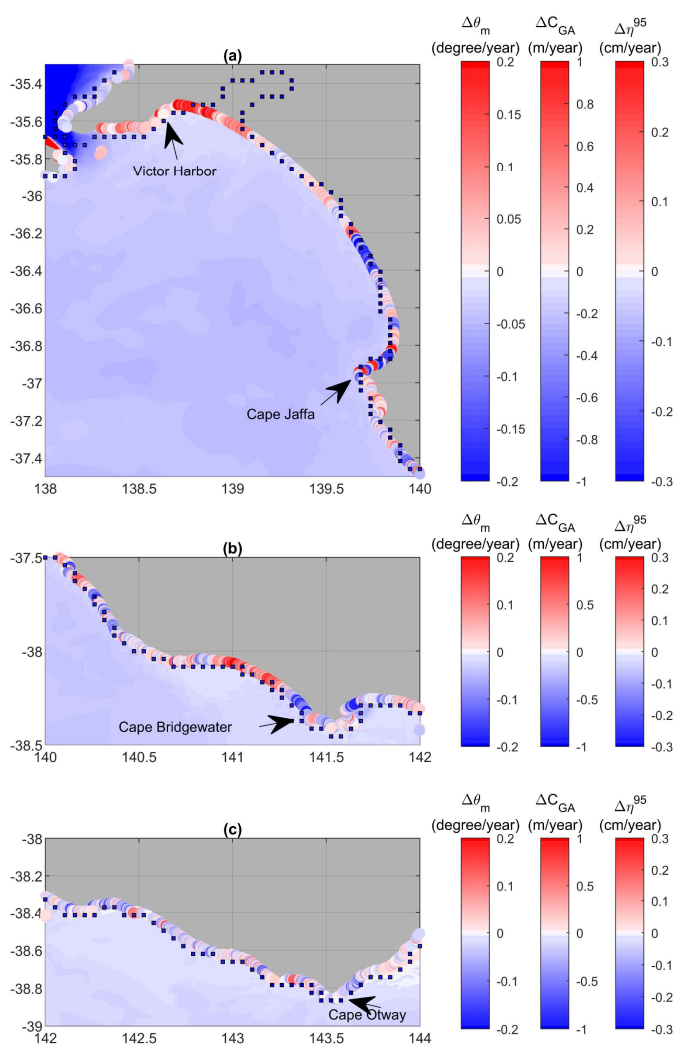


573 Figure 3 d-f: Trends in: wave energy flux, $\Delta C_g E$ shown as colour shaded values over the
574 domain, storm surge, $\Delta \eta^{95}$ shown as a colour shaded squares at coastal model locations and
575 shoreline progradation/recession, ΔC_{GA} shown as colour shaded circles at beach locations.
576 Results shown for sections (d) 144E°-146E°, (e) 146E°-148E° and (f) 148E°-150E°.

577



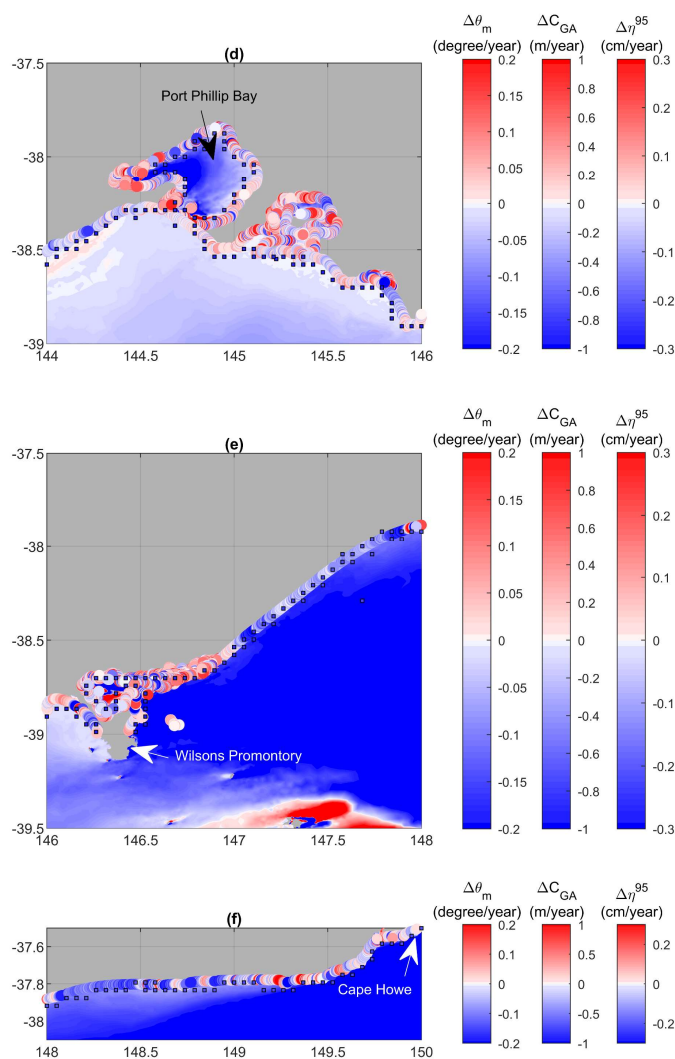
578



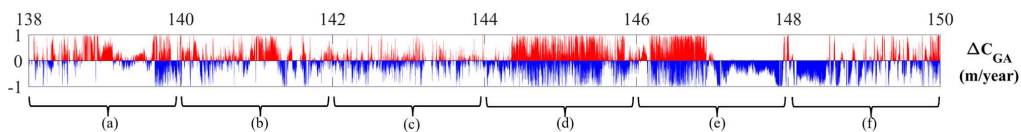
584 Figure 4 a-c: Trends in: mean wave direction, $\Delta\theta_m$ shown as colour shaded values over the
585 domain, storm surge, $\Delta\eta^{95}$ shown as colour shaded squares at coastal model locations and
586 shoreline progradation/recession, ΔC_{GA} shown as colour shaded circles at beach locations.
587 Results shown for sections (a) 138E°-140E°, (b) 140E°-142E°, (c) 142E°-144E°.



588



589 Figure 4 d-f: Trends in mean wave direction, $\Delta\theta_m$ shown as colour shaded values over the
590 domain, storm surge, $\Delta\eta^{95}$ shown as a colour shaded squares at coastal model locations and
591 shoreline progradation/recession, ΔC_{GA} shown as colour shaded circles at beach locations.
592 Results shown for sections (d) 144E°-146E°, (e) 146E°-148E° and (f) 148E°-150E°.



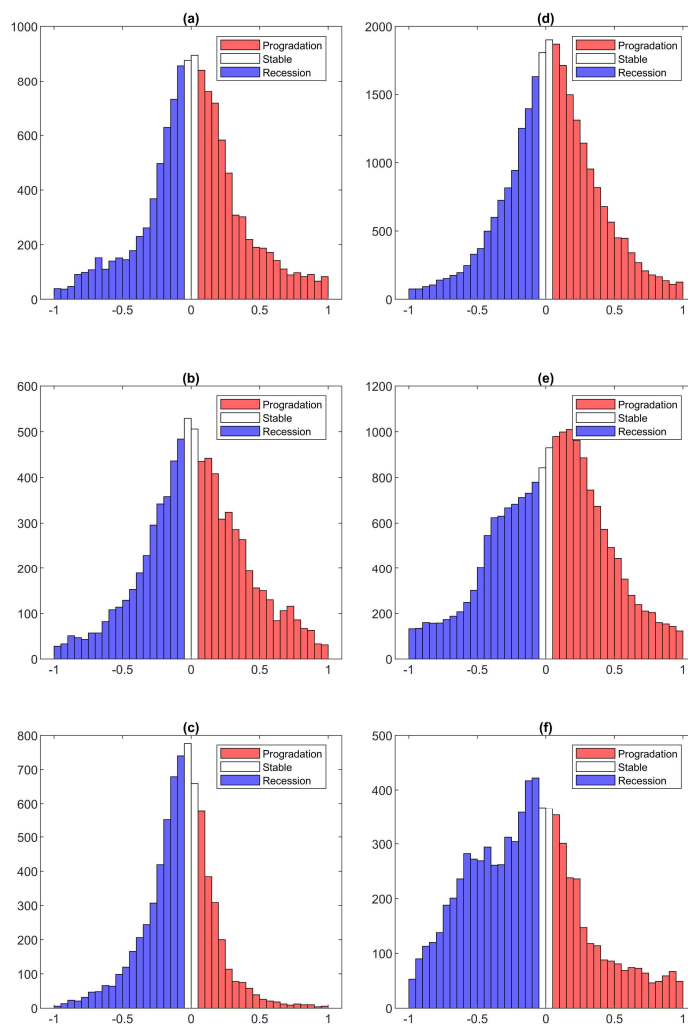
593 Figure 5: Bar chart showing values of progradation (red) and recession (blue), ΔC_{GA} at each
594 coastal location of the Bishop-Taylor, et al. (2021) dataset. Values are shown as a function of the
595 longitude (horizontal axis) and units are m/year. The regions shown in Figure 1 are labelled (a) to
596 (f).

597

598



599



608 Figure 6: Histograms of progradation/recession rates for each of the coastal sections over the
609 period 1988 to 2013. (a) 138E°-140E°, (b) 140E°-142E°, (c) 142E°-144E°, (d) 144E°-146E°, (e)
610 146E°-148E° and (f) 148E°-150E° from west to east.

611